Modelling superradiant amplification of Casimir photons in very low dissipation cavities

2008 J. Phys. A: Math. Theor. 41 164026

(http://iopscience.iop.org/1751-8121/41/16/164026)

IOP PUBLISHING JOURNAL OF PHYSICS A: MATHEMATICAL AND THEORETICAL

J. Phys. A: Math. Theor. **41** (2008) 164026 (9pp) doi:10.1088/1751-8113/41/16/164026

Modelling superradiant amplification of Casimir photons in very low dissipation cavities

J H Brownell[1], **W J Kim**[1] **and R Onofrio**[1,2]

[1] Department of Physics and Astronomy, Dartmouth College, 6127 Wilder Laboratory, Hanover, NH 03755, USA
[2] Dipartimento di Fisica 'Galileo Galilei', Università di Padova, Via Marzolo 8, Padova 35131, Italy

E-mail: roberto.onofrio@dartmouth.edu and roberto.onofrio@pd.infn.it

Received 20 October 2007, in final form 8 January 2008
Published 9 April 2008
Online at stacks.iop.org/JPhysA/41/164026

Abstract

Recent advances in nanotechnology and atomic physics may allow for a demonstration of the dynamical Casimir effect. An array of film bulk acoustic resonators (FBARs) coherently driven at twice the resonant frequency of a high-quality electromagnetic cavity can generate a stationary state of Casimir photons. These are detected using an alkali atom beam prepared in an inverted population of hyperfine states, with an induced superradiant burst producing a detectable radio-frequency signal. We describe here the results of the simulations of the dynamics of superradiance and superfluorescence, with the aim to optimize the parameters for the detectability of Casimir photons. When the superradiant lifetime is shorter than the dissipation time, we find superradiant evolution to be similar in character but dramatically slower than in the usual lossy case.

PACS numbers: 12.20.Fv, 42.50.Pq, 85.85.+j, 42.50.Lc

(Some figures in this article are in colour only in the electronic version)

1. Introduction

Observable effects due to the change in the boundary conditions of quantum fields, like the creation of particles in an expanding universe [1] or the Casimir force [2], provide crucial information on quantum vacuum at the macroscopic level. After the recent results on Casimir forces, with measurements performed in a variety of geometries ranging from the original parallel plane [3, 4] to the sphere plane [5–9] and crossed cylinders [10], there is interest in understanding dissipative effects of vacuum fluctuations, especially its interplay with relativity [11–14]. This dissipation mechanism should induce irradiation of photons, a phenomenon also known as dynamical Casimir effect [15–18]. This can be understood both as the creation

of particles under non-adiabatic changes in the boundary conditions of quantum fields, or as classical parametric amplification with the zero-point energy of a vacuum field mode as input state. In this paper, following on the proposal described in [19], we describe a model for the superradiant amplification scheme with particular emphasis on its dynamics and the optimization of the involved parameters.

2. Generation and detection of Casimir photons

As discussed in [19], under parametric amplification in an electromagnetic cavity an initial state of N_0 photons with frequency within the resonance bandwidth of the fundamental mode of the cavity ω is transformed into a squeezed state with an average number of photons growing in time as [16–18]

$$N_{\mathrm{Cas}}(t) = N_0 \sinh^2(\omega_{\mathrm{mech}}\epsilon t), \tag{1}$$

provided that the parametric resonance condition with a mechanical driving at a frequency $\omega_{\mathrm{mech}} = 2\omega$ is fulfilled. The term $\omega_{\mathrm{mech}}\epsilon$ in the hyperbolic sine function represents the squeezing parameter, with the modulation depth $\epsilon = v/c$, where v is the velocity of the resonator and c is the speed of light. This exponential growth is eventually limited by the photon leakage of the cavity expressed through its quality factor Q, which saturates at the hold time $\tau = Q/\omega$, reaching a maximum photon population

$$N_{\mathrm{Cas}}^{\mathrm{max}} = N_{\mathrm{Cas}}(\tau) = N_0 \sinh^2(2Q\epsilon). \tag{2}$$

Given an initial number of photons in the cavity, which will be attributable to the quantum vacuum at temperatures such that $k_B T \ll \hbar\omega$ (see also [20] for a detailed discussion of the black-body noise), the average number of photons at saturation in equation (2) strongly depends on the product of two parameters, Q and ϵ, which can be on the order of 10^8 and 10^{-8} respectively. The expected saturated power initiated by Casimir emission is

$$P_{\mathrm{Cas}} = N_{\mathrm{Cas}}^{\mathrm{max}} \frac{\hbar\omega}{\tau} \tag{3}$$

and for a 3.0 GHz FBAR resonator and $Q\epsilon \simeq 1$, the saturated power is 3×10^{-22} W, which is too low to be detectable using current technology. This demands the use of an efficient, nearly quantum limited, photon detector in the radio-frequency range. Ultra-sensitive atomic detection schemes can be exploited for detecting Casimir photons by preparing an ensemble of population-inverted atoms in a particular hyperfine state, which for alkali atoms ranges from 0.2 GHz for Li to 9 GHz for Cs, whose transition frequency corresponds to the cavity resonance. An additional amplification process is available in which the weak Casimir signal triggers the stimulated emission of the ensemble of atoms. This effect is a form of superradiance [21, 22]. The hyperfine transition in the ground state occurs through a magnetic dipole interaction, and its natural lifetime in free space is approximately

$$T_1 \approx \frac{4\pi}{\mu_0} \frac{3\hbar}{4\mu_B^2(\omega/c)^3}, \tag{4}$$

where μ_B is the Bohr magneton and μ_0 is the magnetic permeability in vacuum. This natural lifetime in free space is favourably reduced inside a resonant cavity due to the modification of density of states [23, 24],

$$T_1^{\mathrm{cav}} = \frac{4\pi^2}{3Q}\frac{V}{\lambda^3}T_1 \approx \frac{4\pi}{\mu_0}\frac{\hbar V}{8\pi\mu_B^2 Q}, \tag{5}$$

where V is the cavity mode volume. For a few GHz cavity with 1 cm^2 cross-sectional area and $Q = 10^8$, the natural lifetime is reduced by a factor of 10^{10}. In spite of this cavity-enhanced spontaneous rate, the typical hyperfine transition lifetime for the alkali atoms is still impractically long, on the order of $10^3 - 10^5$ s. To shorten this timescale, let us suppose to inject $N_{\rm at}$ excited atoms into the cavity. The Casimir field acts on all atoms, stimulating emission on a time scale of the superradiant lifetime, defined as $T_{\rm SR} = T_1^{\rm cav}/N_{\rm at}$, which is in the millisecond range for $N_{\rm at} \approx 10^8$ or less. An atomic density large enough will then induce a superradiant burst with peak power of $P_{\rm SR} \approx N_{\rm at}\hbar\omega/T_{\rm SR}$, increasing quadratically with the number of atoms. Considering a few GHz resonator with 10^8 atoms and $T_{\rm SR} = 10^{-3}$ s, yields $P_{\rm SR} = 10^{-13}$ W, a billionfold improvement over the power without superradiant amplification as in equation (3).

Spontaneous emission into the cavity mode by the atoms will also trigger a superradiant burst, a process also known as superfluorescence. To distinguish this source of background from the Casimir-stimulated superradiance signal, one may study the temporal intensity envelope of the amplified photons. Both the average delay ($T_{\rm D}$) of the peak intensity from the initial excitation of the atomic population and its fluctuation ($\Delta T_{\rm D}$) are reduced with increasing number of resonant photons $N_{\rm ph}$ initially present [25]:

$$T_{\rm D} = T_{\rm SR}\ln\left(\frac{N_{\rm at}}{1+N_{\rm ph}}\right), \qquad \Delta T_{\rm D} = 2T_{\rm SR}/\sqrt{1+N_{\rm ph}}. \tag{6}$$

It should be noted that these standard results follow when the cavity lifetime is much shorter than the superradiant lifetime. For very high Q, the system of coupled equations of motion must be integrated directly. Tailoring the atomic number can further distinguish the Casimir-stimulated superradiance from superfluorescent pulses. In order for the superradiant pulse to develop fully, the growth rate must exceed any decay process, which is primarily due to Doppler dephasing in the atomic cloud, and the atoms must remain in the interaction region for a time longer than the delay time. A proper choice of $N_{\rm at}$ may suppress superfluorescence relative to Casimir superradiance provided that the atoms will be removed from the cavity after the expected Casimir delay time but prior to the superfluorescence delay ($N_{\rm ph} = 0$ in equation (6)). The superradiant emission can be detected by coupling a power or field detector to the cavity, with response time small enough to resolve one superradiant lifetime. One issue with this direct measurement is the possible reduction of the quality factor of the cavity especially for large coupling efficiency. Micro-bolometers mounted on etched 'spider-webs' have an ultimate sensitivity of 10^{-16} W Hz$^{-\frac{1}{2}}$ in the GHz range [26]. Spectrum analysers are sensitive to sub-fW RF power of kHz bandwidth [27], and the temporal profile of the burst can be reconstructed through vector analysis.

3. Superradiant amplification model

To validate the qualitative estimates in equations (1)–(6), it is necessary to simulate the dynamics of an atomic beam travelling through a low dissipation cavity. We shall discuss here specifically Na atoms initially optically pumped into the $|F = 2, m_F = 2\rangle$ ground state, though the approach is general. Let us consider the second-quantized Hamiltonian with relativistic and hyperfine corrections absorbed into the unperturbed atom term $H^{\rm atom}$ [28],

$$H = \sum_{j=1}^{N} H_j^{\rm atom} - \frac{e}{m_j}\mathbf{p}_j\cdot\mathbf{A}(\mathbf{r}_j) + \frac{e^2}{2m_j}|\mathbf{A}(\mathbf{r}_j)|^2 - \boldsymbol{\mu}_j\cdot\mathbf{B}(\mathbf{r}_j) + \sum_{\lambda}\hbar\omega_\lambda\left(\hat{a}_\lambda^\dagger\hat{a}_\lambda + 1/2\right). \tag{7}$$

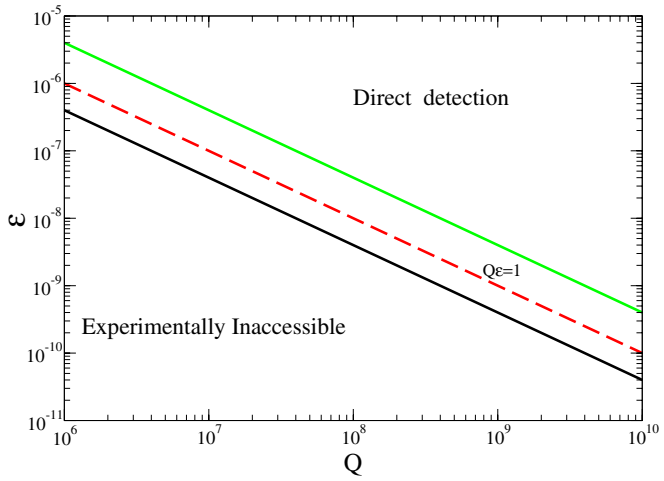

Figure 1. Detectability plot in the $\epsilon - Q$ plane. Depicted from top to bottom are the regions in which direct detection is possible with state-of-art radiofrequency detectors, the region where superradiant amplification extends the range of detection, and the region experimentally inaccessible also to superradiant amplification, with its lower limit due to the speed of micro-bolometers and heterodyne receivers of the current generation. The dashed line corresponds to the benchmark values of Q and ϵ satisfying $Q\epsilon = 1$ which are at the edge of current technology of superconducting cavities and nanotechnology.

The subscripts j and λ are the atom and field mode index, respectively, ω_λ is the mode angular frequency. The fields $\mathbf{A}(\mathbf{r}_j)$ and $\mathbf{B}(\mathbf{r}_j) = \nabla \times \mathbf{A}(\mathbf{r}_j)$ are defined in terms of field profiles functions $\mathbf{U}(\mathbf{r}_j)$ and creation and annihilation operators $(a, a^\dagger)$ as

$$\mathbf{A}(\mathbf{r}_j) = \sum_\lambda \sqrt{\frac{\hbar}{2\epsilon_0 \omega_\lambda}} \left[\mathbf{U}_\lambda(\mathbf{r}_j)\hat{a}_\lambda + \mathbf{U}^*_\lambda(\mathbf{r}_j)\hat{a}^\dagger_\lambda\right] \tag{8}$$

$$\mathbf{B}(\mathbf{r}_j) = i \sum_\lambda \sqrt{\mu_0 \hbar \omega_\lambda / 2} \left[\hat{\mathbf{k}}(\mathbf{r}_j) \times \mathbf{U}(\mathbf{r}_j)\hat{a}_\lambda - \hat{\mathbf{k}}(\mathbf{r}_j) \times \mathbf{U}(\mathbf{r}_j)^* \hat{a}^\dagger_\lambda\right], \tag{9}$$

where the field profile functions form an orthonormal set and the $a, a^\dagger$ operators fulfil the usual commutation relationships,

$$\int \mathrm{d}^3 r\, \mathbf{U}_\lambda(\mathbf{r}_j)\mathbf{U}^*_{\lambda'}(\mathbf{r}_j) = \delta_{\lambda\lambda'};\ \left[\hat{a}_\lambda, \hat{a}^\dagger_{\lambda'}\right] = \delta_{\lambda\lambda'};\ [\hat{a}_\lambda, \hat{a}_{\lambda'}] = \left[\hat{a}^\dagger_\lambda, \hat{a}^\dagger_{\lambda'}\right] = 0. \tag{10}$$

Given no initial population on an upper state of an electric dipole transition and no initial or applied field resonant with the same, the second and the third terms in equation (7) can be ignored and each atom evolves only within the manifold of ground hyperfine states. The atomic Hamiltonian then can be represented by an 8×8 matrix and the Heisenberg equations of motion derived. To simplify the discussion, let us assume a cylindrically symmetric cavity with field propagation ($\hat{\mathbf{k}}$) primarily along the cavity axis ($\hat{\mathbf{z}}$), with quantization axis along the cavity axis, so that the active modes will be circularly polarized. If we also assume the ideal case where the Na atoms are prepared in the $|F = 2, m_F = 2\rangle$ state, then only the $|F = 2, m_F = 2\rangle - |F = 1, m_F = 1\rangle$ transition will be active and the Hamiltonian can be

reduced to

$$H = \sum_{j=1}^{N} \begin{pmatrix} \hbar\left(\Omega - \mathbf{k}\cdot\mathbf{v}_j\right) & \mu_- B_+(\mathbf{r}_j) \\ \mu_+ B_-(\mathbf{r}_j) & 0 \end{pmatrix} + \sum_{\lambda} \hbar\omega_\lambda \left(\hat{a}_\lambda^\dagger \hat{a}_\lambda + 1/2\right), \tag{11}$$

using the standard notation for polarization,

$$\boldsymbol{\mu} = \mu_+ \hat{\boldsymbol{\varepsilon}}_+ + \mu_- \hat{\boldsymbol{\varepsilon}}_- + \mu_z \hat{\mathbf{z}}, \tag{12}$$

and likewise for $\mathbf{B}$ and $\mathbf{U}$ with $\hat{\boldsymbol{\varepsilon}}_\pm = (\hat{\mathbf{x}} \pm \hat{\mathbf{y}})/\sqrt{2}$. The hyperfine transition resonance frequency $\Omega \equiv \left\{H_{22}^{\text{atom}} - H_{11}^{\text{atom}} - \mu_z^{F=2} B_z^{DC}(\mathbf{r}_j) + \mu_z^{F=1} B_z^{DC}(\mathbf{r}_j)\right\}/\hbar$ can be tuned with an applied DC magnetic field along the quantization axis. Furthermore, given $\mu_+ = \mu_- \equiv \mu$, it is convenient to define the Rabi frequency coefficient $\chi_\lambda(\mathbf{r}_j) \equiv \mu\sqrt{\mu_0 \hbar\omega_\lambda/2}\, U_\lambda(\mathbf{r}_j)/\hbar$ and employ Pauli matrix operators in writing the Hamiltonian as

$$H = \sum_{\lambda} \hbar\omega_\lambda \left(\hat{a}_\lambda^\dagger \hat{a}_\lambda + 1/2\right) + \sum_{j=1}^{N} \left\{ \frac{1}{2}\hbar(\Omega - \mathbf{k}\cdot\mathbf{v}_j)(\hat{\sigma}_{0j} + \hat{\sigma}_{zj}) \right.$$
$$\left. - \mathrm{i}\hbar \sum_{\lambda} \left[\chi_\lambda(\mathbf{r}_j)\hat{\sigma}_{+j}\hat{a}_\lambda - \chi_\lambda^*(\mathbf{r}_j)\hat{\sigma}_{-j}\hat{a}_\lambda^\dagger\right] \right\}. \tag{13}$$

Here it is understood that the field operators represent only right circular polarization and the atom operators act only on operators of the same atom. The Heisenberg equations of motion resolve to

$$\dot{\hat{\sigma}}_{zj} = -2 \sum_{\lambda} \left\{ \chi_\lambda(\mathbf{r}_j)\hat{\sigma}_{+j}\hat{a}_\lambda + \chi_\lambda^*(\mathbf{r}_j)\hat{\sigma}_{-j}\hat{a}_\lambda^\dagger \right\} \tag{14}$$

$$\dot{\hat{\sigma}}_{+j} = i(\Omega - \mathbf{k}\cdot\mathbf{v}_j)\hat{\sigma}_{+j} + \sum_{\lambda} \chi_\lambda^*(\mathbf{r}_j)\hat{\sigma}_{zj}\hat{a}_\lambda^\dagger \tag{15}$$

$$\dot{\hat{a}}_\lambda = -i\omega_\lambda \hat{a}_\lambda + \sum_{j=1}^{N} \chi_\lambda^*(\mathbf{r}_j)\hat{\sigma}_{-j}. \tag{16}$$

Note that total energy and excitation number are conserved in a lossless system as well as the Bloch vector length. Optical losses from the cavity can be included by adding a negative imaginary loss rate, $\Gamma = \omega_\lambda/2Q$, to the mode frequency. In assuming a constant loss rate, we neglect the back action of the incoming atoms on the frequency and the quality factor of the cavity mode, an approximation which could be relaxed only by handling the complete cavity-atom problem. The operators can be factored as $\hat{a}_\lambda = \tilde{a}_\lambda\, \mathrm{e}^{-\mathrm{i}\omega_\lambda t}$ and $\hat{\sigma}_{\pm j} = \tilde{\sigma}_{\pm j}\, \mathrm{e}^{\pm\mathrm{i}(\Omega - \mathbf{k}\cdot\mathbf{v}_j)t}$, isolating the variable envelopes which are easier to integrate numerically.

Furthermore, if the cavity lifetime is much shorter than the superradiant lifetime ($1/\Gamma \ll T_{\text{SR}}$), then it is convenient to first integrate equation (16) approximately through a Green's function method by assuming the atom does not evolve significantly within one cavity lifetime [28],

$$\hat{a}_\lambda(t) \approx \tilde{a}_\lambda(0)\, \mathrm{e}^{-(\mathrm{i}\omega_\lambda + \Gamma)t} + \sum_{j=1}^{N} \chi_\lambda^*(\mathbf{r}_j) g_{\lambda j}(t)\hat{\sigma}_{-j}, \qquad \text{for} \quad \Gamma T_{SR} \gg 1, \tag{17}$$

where $g_{\lambda j}(t) \equiv (1 - \exp[(-\mathrm{i}\Delta_{\lambda j} - \Gamma)t])/(\mathrm{i}\Delta_{\lambda j} + \Gamma)$ with detuning between cavity and atom resonance is defined as $\Delta_{\lambda j} \equiv \omega_\lambda - (\Omega - \mathbf{k}\cdot\mathbf{v}_j)$. Essentially, each atom responds to the emission from all atoms accumulated over one cavity lifetime. This result can then

be inserted into equations (14) and (15), defining the detuning between atom resonances $\Delta_{ij} \equiv \mathbf{k} \cdot (\mathbf{v}_i - \mathbf{v}_j)$, to yield

$$\dot{\tilde{\sigma}}_{zj} = -2 \sum_{\lambda} \left\{ \chi_\lambda(\mathbf{r}_j)\, \mathrm{e}^{(-\mathrm{i}\Delta_{\lambda j} - \Gamma)t} \tilde{\sigma}_{+j} \tilde{a}_\lambda(0) + \chi_\lambda^*(\mathbf{r}_j)\, \mathrm{e}^{(\mathrm{i}\Delta_{\lambda j} - \Gamma)t} \tilde{\sigma}_{-j} \tilde{a}_\lambda^\dagger(0) \right.$$
$$\left. + \sum_{i=1}^{N} \left\{ \chi_\lambda(\mathbf{r}_j) \chi_\lambda^*(\mathbf{r}_i) g_{\lambda i}(t)\, \mathrm{e}^{-\mathrm{i}\Delta_{ij} t} \tilde{\sigma}_{+j} \tilde{\sigma}_{-i} + \chi_\lambda^*(\mathbf{r}_j) \chi_\lambda(\mathbf{r}_i) g_{\lambda i}^*(t)\, \mathrm{e}^{\mathrm{i}\Delta_{ij} t} \tilde{\sigma}_{-j} \tilde{\sigma}_{+i} \right\} \right\}, \tag{18}$$

$$\dot{\tilde{\sigma}}_{+j} = \sum_{\lambda} \left\{ \chi_\lambda^*(\mathbf{r}_j)\, \mathrm{e}^{(-\mathrm{i}\Delta_{\lambda j} - \Gamma)t} \tilde{\sigma}_{zj} \tilde{a}_\lambda(0) + \sum_{i=1}^{N} \chi_\lambda^*(\mathbf{r}_j) \chi_\lambda(\mathbf{r}_i) g_{\lambda i}^*(t)\, \mathrm{e}^{\mathrm{i}\Delta_{ij} t} \tilde{\sigma}_{zj} \tilde{\sigma}_{-i} \right\}. \tag{19}$$

The field intensity, square of equation (17), can then be produced from the atomic state by first numerically integrating these reduced equations. The terms linear in $\tilde{a}_\lambda(0)$ represent the negligible action by the initial field. The quadratic terms involve feedback from all other atoms that generates superradiance. Note that on resonance ($\Delta_{\lambda j} = 0$) we arrive at the expected time scale, for $t \gg 1/\Gamma$, through the coefficient

$$\chi_\lambda^*(\mathbf{r}_j) \chi_\lambda(\mathbf{r}_i) g_{\lambda j}(t) = \frac{\mu_0 \mu^2 \omega_\lambda}{2\hbar V_\lambda} \frac{2Q}{\omega_\lambda} V_\lambda U_\lambda^*(\mathbf{r}_j) U_\lambda(\mathbf{r}_i) = \frac{1}{2T_1^{\mathrm{cav}}} V_\lambda U_\lambda^*(\mathbf{r}_j) U_\lambda(\mathbf{r}_i). \tag{20}$$

For significant amplification, the number of interacting atoms must be large and it becomes prohibitively difficult to solve the $2N$ coupled equations of motion. Instead one can dice the atomic distribution in phase space into finite close-packed cells so that the number of cells is computationally feasible and the pertinent distribution and field profile features are retained. These constraints typically imply that the number of atoms per cell is at least ten. In this case, the correlation between the atomic population and photon number is inconsequential (i.e. atom stimulation rate is not significantly limited by the stored energy) and the expectation value of the operator products can be factored as $\langle \tilde{\sigma}_{+j} \tilde{a}_\lambda \rangle \approx \langle \tilde{\sigma}_{+j} \rangle \langle \tilde{a}_\lambda \rangle$. The sum over atoms can then be replaced with the multiple sum over cell indices,

$$\sum_{j=1}^{N} f_j(\mathbf{r}_j, \mathbf{v}_j) \to \sum_i \sum_j \sum_k \sum_l N_{ijkl} f_{ijkl}\left(\langle x \rangle_i^{\mathrm{cell}}, \langle y \rangle_j^{\mathrm{cell}}, \langle z \rangle_k^{\mathrm{cell}}, \langle v_\parallel \rangle_l^{\mathrm{cell}} \right), \tag{21}$$

provided the atom position and velocity are replaced with the mean cell position $\mathbf{r}_j \to \langle \mathbf{r} \rangle_{\mathrm{cell}}$ and velocity $\mathbf{v}_j \to \langle \mathbf{v} \rangle_{\mathrm{cell}}$ and the atom operators now represent the typical atom in the cell. The number of atoms in cell $\{i, j, k, l\}$ is designated as N_{ijkl}, and only the parallel component of velocity is relevant. The cellular equations of motion can then be numerically integrated given the initial expectation values, atom and field distribution, atom resonance and moment, and field resonance. Collisions can be simulated by introducing a random phase factor, depending on the number of atoms in the cell, to the atom operators between time steps. Assuming an initially inverted atomic population, superfluorescence can be simulated by assuming zero photons present and an initial 'tipping angle', $\langle \tilde{\sigma}_{zj} \rangle (t = 0) = 2/\sqrt{N_{\mathrm{at}}}$, of the Bloch vector representing spontaneous atom state fluctuations [25]. Likewise, Casimir-stimulated superradiance may be simulated by assuming the same tipping angle and initial field amplitude $\langle \tilde{a}_\lambda \rangle (t = 0) = \sqrt{N_{\mathrm{Cas}}^{\mathrm{max}}}$, given the parametric amplification process generates a coherent state of the field.

4. Discussion of numerical results and conclusions

The coupled equations of motion, equations (14)–(16), were integrated by Runge–Kutta method for a small sample of Na atoms traversing a planar-concave optical cavity through the

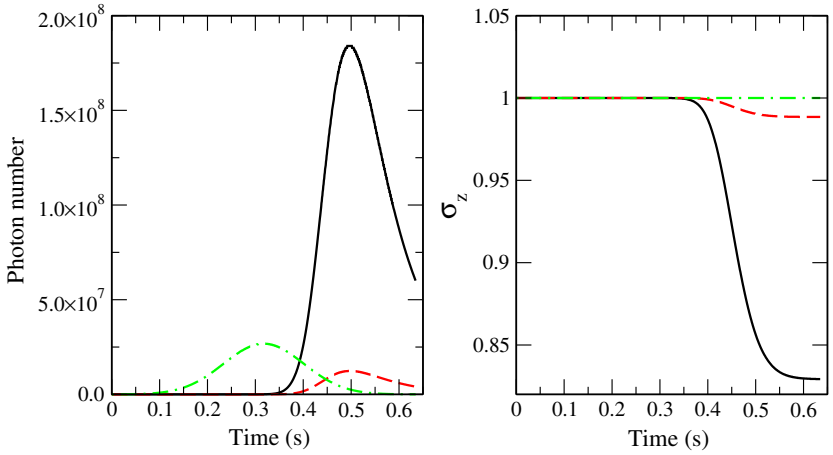

Figure 2. Dynamics of superradiant amplification of Casimir photons (assumed in the number of 10^2) and competition with superfluorescence. On the left plot, the superradiant emitted photons (solid line, black) compared to the superfluorescence in the absence of Casimir photons (dotted line, red) are depicted versus time. The dot-dashed curve in green indicates the field strength profile felt by the atoms. On the right plot, the atomic inversion populations for superradiant (solid line, black) and superfluorescence (dotted line, red) are also plotted versus time. The dot-dashed curve in green indicates the degree of conservation of the Bloch vector length during the simulation. The simulation is performed for Na atoms with $Q = 10^9$, $N_{\rm at} = 10^{10}$, 1 m s^{-1} atom velocity, 10 mK temperature. The relevant time scales are $1/\Gamma = 0.18$ s, $T_1^{\rm cav} = 10^6$ s, $T_{\rm SR} = 10^{-4}$ s and Doppler dephasing time $T_2^* = 63$ ms.

diameter at 10% of the cavity length height above the planar mirror. The cavity is tuned so that the first longitudinal TEM00 Gaussian mode is resonant with the atoms. The atom distribution was divided into five cells varying in velocity symmetrically about the mean speed. The number of atoms, cavity quality, atom mean speed, atom transverse temperature (i.e. velocity spread) and initial photon population were varied to identify promising configurations and sensitivity of the superradiant output. We found that there is a range of configurations, corresponding to the high end of experimental feasibility, that achieve a high degree of discrimination between the Casimir-stimulated superradiant and the superfluorescent emission. In figure 2, we show the typical emission profile (left panel) and atomic inversion population (right panel). As suggested above, the superfluorescent emission is suppressed if the atoms leave the field mode region before its amplification can develop. Even a single photon in the cavity can generate a signal 60% above the superfluorescent background. Atom numbers too high or too low, depending primarily on Q and atom speed, allow both cases to develop fully or very little, respectively. Superradiant amplification is quite effective for sufficiently high gain, easing RF detector sensitivity requirements. The gain is very sensitive to $N_{\rm at}$ and Q and the atom transit time ($\propto 1/v_{\rm at}$). Also, the strong discrimination in amplification indicated by η in table 1 implies that the detector response time need not be a significant constraint, as would be the case if the delay time should be measured. The discrimination ratio is fairly insensitive to temperature, suggesting that a slowed beam rather than a trap could be used, providing larger $N_{\rm at}$. Strong amplification necessarily results in a large fraction of the atoms driven to their ground state. Therefore, probing the atomic beam ground state through D-line excitation after it transits the cavity, as we had proposed in [19], is a viable option that avoids detector losses in the cavity. The high values of $N_{\rm at}$ and Q would be eased significantly if the number

Table 1. Configurations yielding effective discrimination between Casimir superradiant signals and superfluorescence noise. The degree of discrimination is indicated by the ratio of the peak intensity for the SR case to the SF case (η) and the analogous ratio of the ground-state population after the atoms exit the cavity (ξ). The ground-state population of the atoms near resonance is given by $\rho_{\rm gnd}^{\rm SR} = (1 - \langle\sigma_z(\Delta \approx 0)\rangle)/2$. The superradiant lifetime for these cases is in the range of $T_{\rm SR} = 1 - 100\ \mu$s, roughly 10^3 times less than the cavity decay time, implying $\Gamma T_{\rm SR} \ll 1$.

$N_{\rm max}^{\rm cas}$	$N_{\rm at}$	$v_{\rm at}$ (m s^{-1})	Q	$T_{\rm at}$ (K)	$\langle a^\dagger a\rangle$ (peak)	η	$\rho_{\rm gnd}^{\rm SR}$ (%)	ξ
10^2	1×10^{10}	1	1×10^9	0.01	1.8×10^8	15	8.5	15
10^2	1×10^{10}	1	2×10^9	0.01	9.6×10^8	26	34	26
10^2	1×10^{10}	1	4×10^9	0.01	2.1×10^9	31	39	20
10^2	5×10^9	1	1×10^9	0.01	5.1×10^5	14	0.049	14
10^2	2×10^{10}	1	1×10^9	0.01	8.2×10^9	1.2	49	1.8
10^2	4×10^{10}	1	1×10^9	0.01	2.4×10^{10}	1.0	23	7.3
10	1×10^{10}	1	1×10^9	0.01	4.5×10^7	3.6	2.1	3.6
1	1×10^{10}	1	1×10^9	0.01	2.0×10^7	1.6	0.95	1.6
10^2	1×10^{10}	1	1×10^9	0.1	1.0×10^8	15	4.6	15
10^2	1×10^{10}	1	1×10^9	1	9.4×10^7	15	4.3	15
10^2	1×10^{10}	1	1×10^9	10	9.3×10^7	15	4.3	15
10^2	2×10^{10}	2	1×10^9	0.01	6.3×10^6	30	0.11	30
10^2	2×10^{10}	2	2×10^9	0.01	1.8×10^7	45	0.26	45
10^2	2×10^{10}	2	4×10^9	0.01	3.0×10^7	56	0.4	56
10^2	1×10^{10}	2	1×10^9	0.01	6.7×10^4	28	2.5×10^{-3}	28
10^2	4×10^{10}	2	1×10^9	0.01	5.4×10^9	22	48	22
10^2	1×10^{11}	10	1×10^9	0.01	4.2×10^4	760	7×10^{-5}	680
10^2	4×10^{11}	10	1×10^9	0.01	2.9×10^8	650	0.11	650
10^2	1×10^{12}	10	1×10^9	0.01	8.7×10^{11}	42	25	8.6
10^2	1×10^{11}	10	2×10^9	0.01	5.3×10^4	840	8.3×10^{-5}	760
10^2	1×10^{11}	10	4×10^9	0.01	6.0×10^4	890	9.1×10^{-5}	810

of initial Casimir photons is increased. Equation (2) implies $N_{\rm max}^{\rm Cas} = 0.7, 6, 370, 10^6$ for $Q\epsilon = 0.5, 1, 2, 3$. The rapid change in initial photon population $N_{\rm max}^{\rm Cas}$ due to Q for a given modulation mechanism is not taken into account in table 1. One caveat to the above results and discussion is that the computed time for the superradiant burst to develop is far longer than the standard prediction, equation (6). The configurations tested imply $\Gamma T_{\rm SR} \ll 1$, in violation of the approximation condition under which equation (6) was derived. Indeed, the reduced equations of motion, equations (17) and (19), were quite unstable under these conditions. As we have shown, the standard result develops naturally from the general theory given a lossy environment. The transition to a low loss environment appears to have a dramatic effect delaying the field growth. We are currently studying the origin and domain of validity of this effect.

Acknowledgments

RO acknowledges partial support by the NSF through the Institute for Theoretical Atomic and Molecular Physics at Harvard University and the Smithsonian Astrophyiscal Observatory.

References

[1] Schrödinger E 1939 *Physica* **6** 899
[2] Casimir H B G 1948 *Proc. K. Ned. Akad. Wet.* B **51** 793

[3] Sparnaay M J 1958 *Physica* **24** 751
[4] Bressi G, Carugno G, Onofrio R and Ruoso G 2002 *Phys. Rev. Lett.* **88** 041804
[5] van Blokland P H G M and Overbeek J T G 1978 *J. Chem. Soc. Faraday Trans.* I **74** 2637
[6] Lamoreaux S K 1997 *Phys. Rev. Lett.* **78** 5
[7] Mohideen U and Roy A 1998 *Phys. Rev. Lett.* **81** 4549
[8] Iannuzzi D, Lisanti M, Munday J and Capasso F 2005 *Solid State Commun.* **135** 618
[9] Decca R S *et al* 2005 *Ann. Phys.* **318** 37
[10] Ederth T 2000 *Phys. Rev.* A **62** 062104
[11] Moore G T 1970 *J. Math. Phys.* **11** 2679
[12] Fulling S A and Davies P C W 1976 *Proc. R. Soc. Lond.* A **348** 393
[13] Jaekel M-T and Reynaud S 1997 *Rep. Prog. Phys.* **60** 863
[14] Lambrecht A, Jaekel M-T and Reynaud S 1996 *Phys. Rev. Lett.* **77** 615
[15] Barton G, Dodonov V V and Man'ko V I (ed) 2005 *J. Opt.* B **7**
[16] Dodonov V V and Klimov A B 1996 *Phys. Rev.* A **53** 2664
[17] Plunien G, Schützhold R and Soff G 2000 *Phys. Rev. Lett.* **84** 1882
[18] Crocce M, Dalvit D A R and Mazzitelli F D 2001 *Phys. Rev.* A **64** 013808
[19] Kim W-J, Brownell J H and Onofrio R 2006 *Phys. Rev. Lett.* **96** 200402
[20] Kim W-J, Brownell J H and Onofrio R 2007 *EPL* **78** 21002
[21] Benedict M G *et al* 1996 *Superradiance: Multiatomic Coherent Emission* (Bristol: Institute of Physics Publishing)
[22] Gross M and Haroche S 1982 *Phys. Rep.* **93** 301
[23] Purcell E M 1946 *Phys. Rev.* **69** 681
[24] Goy P, Raymond J M, Gross M and Haroche S 1983 *Phys. Rev. Lett.* **50** 1903
[25] Goy P *et al* 1982 *Phys. Rev.* A **27** 2065
[26] Turner A D *et al* 2001 *Appl. Opt.* **40** 4921
[27] Agilent Technologies, Inc., Palo Alto, CA
[28] Allen L and Eberly J H 1987 *Optical Resonance and Two-level Atoms* (New York: Dover)